Available online at www.sciencedirect.com

ScienceDirect

Solar Energy 115 (2015) 243–254

SOLAR ENERGY

www.elsevier.com/locate/solener

Optimal energy control of grid tied PV–diesel–battery hybrid system powering heat pump water heater

Sam M. Sichilalu *, Xiaohua Xia

Centre of New Energy Systems, Department of Electrical, Electronic and Computer Engineering, University of Pretoria, Pretoria 0002, South Africa

Received 17 November 2014; received in revised form 21 January 2015; accepted 1 February 2015

Communicated by: Associate Editor Mukund R. Patel

Abstract

This paper develops an optimal control strategy for power dispatch of the grid-tied photovoltaic (PV)–battery–diesel system to power heat pump water heaters (HPWH). The system consists of the PV modules, grid, battery, HPWH, diesel generator (DG) and other domestic appliances. The PV can simultaneously feed in the excess power to the grid and supply the loads. The battery is used as storage of cheaper-to-buy off-peak grid energy, dependent on the time-of-use (TOU) electricity tariff, while the DG is a backup power source to the HPWH. The objective function of the model is to minimize energy and fuel cost while maximizing PV energy trade-off for incentives. The TOU is an important control parameter in this model. The power flows from each power source are the control variables. The optimal control shows a great potential to realize a practical net zero-energy building and demand side management. This model meets both the technical and operational constraints. A case study is done based on a 3×16 kW HPWH installed at a Pretoria Hotel in South Africa. Simulations run over a year on selected seasonal dates using the actual measured demand of the HPWH. The optimal control problem is solved using a mixed integer non-linear program and the results show how TOU affects the power dispatch to the HPWH. The energy and cost savings are presented in this paper.

Keywords: Heat pump water heater; Optimal control; Photovoltaic; Net zero-energy building; Diesel generator; Mixed integer nonlinear program

1. Introduction

A heat pump water heater (HPWH) operates on the principle of the refrigerant cycle. The electrical energy drives the compressor (Hepbasli and Kalinci, 2009), which compresses the refrigerant (working fluid) inside the constant volume. The HPWH has advantage over the storage tank water heaters (geysers) because of its combined energy-harvesting technique, it collects the surrounding ambient energy and increases it through the compression action. The HPWH consumes only one unit of electrical energy to produce three units of thermal energy, whereas geysers use three units of electrical energy to yield the same quantity as the HPWH. HPWH uses two thirds less electrical energy owing to its coefficient of performance (COP). This huge energy saving has made heat pumps gain wider application (Verhelst et al., 2012) in both space and water heating. Research on optimal sizing and maximization of ambient energy harvesting from the surrounding environment using HPWHs continues. Many researchers (Ahmad et al., 2013; Chow et al., 2012; Kjellsson et al., 2010; Ji et al., 2005; Zhang et al., 2007) have presented models that can efficiently recover the natural surrounding ambient energy through a combination of techniques. Esen

* Corresponding author. Tel.: +27 12 420 6767; fax: +27 12 362 5000.
E-mail addresses: Sam.Sichilalu@up.ac.za, sichgroup@yahoo.com (S. M. Sichilalu).

http://dx.doi.org/10.1016/j.solener.2015.02.028
0038-092X/

Nomenclature

P_i	control variable, which is the power flow in the ith branch (kW)
min and *max*	minimum and maximum of the variable
R	South African rands (ZAR)
p	TOU electricity price (R/kW h)
N	total number of sampling intervals
t_s and k	sampling time (h) and kth sampling interval
ω	weighting factor
p_c	photovoltaic feed-in tariff (R/kW h)
P_{hp}	heat pump water heater power demand (kW)
COP	coefficient of performance
P_{dl}	domestic appliances power demand (kW)
P_{pv}	photovoltaic power output (kW)
$B_c(t)$	battery capacity at every given time t in (kW h)
η_c	battery charging efficiency
η_d	battery discharging efficiency
$B_c(0)$	initial state of energy of the battery (kW h)
SOE	battery state of energy (kW h)
σ	battery self-discharged factor
B_c^{max}	maximum battery rated capacity in (A h)
a, b and c	diesel generator coefficients
C_f	diesel fuel price (R/l)
F	diesel generator fuel consumption in (l/h)
Z_m	experimental measured values
A_m	true or accepted value
$\sigma_{m,meas}$	standard deviation
MINLP	Mixed Integer Nonlinear Program

et al. (2007, 2006) extensively investigated the effects of the ground-sourced and air-sourced heat pump systems and carried out the techno-economical analysis. These efforts are directed at improving the COP of the HPWHs.

Rahman et al. (2010) mentioned that the energy consumption of buildings accounts for approximately 42% in developed countries. The energy consumption ratio[1] domestic buildings is about 60.51% for space heating and 23.60% for water heating in most developed countries. Therefore, energy-efficient equipment is necessary at building level in order to reduce consumption and greenhouse gas emission. HPWHs could provide solutions for energy reduction and demand side management (DSM) if optimally integrated with distributed renewable energy resources (DREs). However, there are still technological challenges (Chua et al., 2010) in system design and integration. The initial cost remains a major draw-back (Rousseau and Greyvenstein, 2000) in the application of HPWHs, especially in developing countries. Their application in developing countries is still uneconomical because of various technological challenges and policies; for example, in South Africa the market penetration (Rousseau and Greyvenstein, 2000) of HPWHs is just slightly above 16%.

In order to save energy substantively at building level, a multi-directional holistic approach is needed to achieve a practical positive-energy building or net zero-energy building (NZEB). These DREs can either be on/off-site powering the entire building (zero energy buildings) or grid-connected referred to as NZEBs. The collective effort required to turn a new or existing buildings into an NZEB involves proper selection of an appropriate technology, application of optimal control in DREs, usage of energy-efficient equipment, green building materials and an effective energy policy (Trianni and Cagno, 2012). Most authors (Marszal et al., 2011; Scognamiglio and Røstvik, 2013; Torcellini and Crawley, 2006) agree that a multi-directional approach to energy saving will conquer the existing challenges in NZEBs. Currently more efforts are put into the development and application (Khudhair and Farid, 2004) of phase change materials (PCMs) (Esen, 2000), that store the thermal energy and releases it to the surrounding medium whenever there is a temperature imbalance. In buildings PCMs are used to store energy which is captured from the solar radiation and is used to maintain the interior temperatures (Infield et al., 2004; Santamouris, 2014) and save energy demanded by heating, ventilation, and air-conditioning (HVAC) systems. In Esen (2000) the water storage tank with PCMs is integrated with solar thermal collectors, the system stored the solar energy in the PCMs submerged into the water tank. The PCMs acted later as the latent energy source for the heat pump, especially during low or no solar energy from the collectors.

On/off-site DREs integration into buildings and small communities is a promising technology for DSM. The building will be able to generate power to meet its own demand and trade-off to the grid. Various hybrid DREs systems are extensively explained in Tazvinga et al. (2013), Ashok (2007), Esen and Yuksel (2013), Dufo-Lopez and Bernal-Agustín (2005), Dagdougui et al. (2012) and Ekren and Ekren (2008). However, most of the success achieved is in the areas of optimal life cycle costing and system sizing. Research into the application of an optimal control strategy to achieve the right energy mix between the grid and DREs dependent on the time-of-use electricity tariff (TOU) to power HPWHs is in the infancy stage. HPWHs are some of the energy-efficient tools that can be employed on the DSM (Setlhaolo et al., 2014). DREs feed-in or trade-off to the grid, as well as the application of energy-efficient equipment, such as HPWHs, could attract incentives in certain countries.

[1] http://www.dti.gov.uk/energy/inform/.

This paper proposes a combined model that could achieve a practical NZEB. Ikegami et al. (2012) attempted to develop an ideal model using the HPWH and electrical vehicles to manage power utility maximum demand. This paper proposes the first attempt at optimal energy control of a grid-tied photovoltaic (PV) diesel generator to power HPWHs and the domestic load, modeling a practical NZEB. Among the other contributions of this paper is a proposed new battery usage model, which works as storage of cheaper-to-buy off-peak grid energy and the application of a mixed nonlinear program (MINLP) to solve the real NZEB problem. This model may be adopted to provide optimal DRE trade-off to home owners who intend to turn their dwelling into an energy-positive building based on the weighting factor in the cost function and desired effects.

This paper is structured as follows: Section 2 is the mathematical formulation, Section 3 is the simulation results and discussion. The last part, Section 4, is the conclusion.

2. Mathematical formulation

2.1. Schematic model layout

The optimal control (OC) strategy schematic diagram shown in Fig. 1 consists of the utility power grid, PV modules, battery, diesel generator, HPWH and domestic load. The grid can supply power $P_1(t)$ directly through a switch $u_1(t)$ to the HPWH, while $P_2(t)$ is used to charge the battery and $P_3(t)$ supplies the domestic load. This paper presents a new battery connection model; unlike many conventional models found in literature (Rodolfo Dufo-LoŽpez, 2008; Kim et al., 2008; Ikegami et al., 2010), the battery is used to store cheaper-to-buy off-peak grid energy. The stored off-peak energy is then made available during peak TOU tariff hours to supplement the PV and DG supplies to the HPWH. In situations where the battery, DG and PV power are uneconomical or insufficient to meet the demand, the OC switches on $u_1(t)$ enabling direct grid supply to the HPWH. The DG supplies power P_8 to HPWH only, in periods when it is uneconomical to use grid energy. The PV modules can supply power to all the loads and at the same time feed into the grid, $P_5(t)$ supplies the HPWH, $P_6(t)$ supplies the domestic load and $P_4(t)$ is the excess PV power sold to the grid.

The optimal scheduling decides the amount of excess PV energy to be sold to the grid, mainly based on the weighting factor to maximize the net benefit of the customer. The PV energy trade-off and usage of the HPWH attract incentives in the case study, though these are not considered in this paper. The DG is a backup power supply in the periods when the PV or grid energy is unavailable or uneconomical depending on the TOU.

2.2. Sub-models

2.2.1. Diesel generator

The diesel generator has a typical maximum fuel efficiency of 3 kW h/l when it is running above 80% (Ashari and Nayar, 1999) and the lowest fuel efficiency when

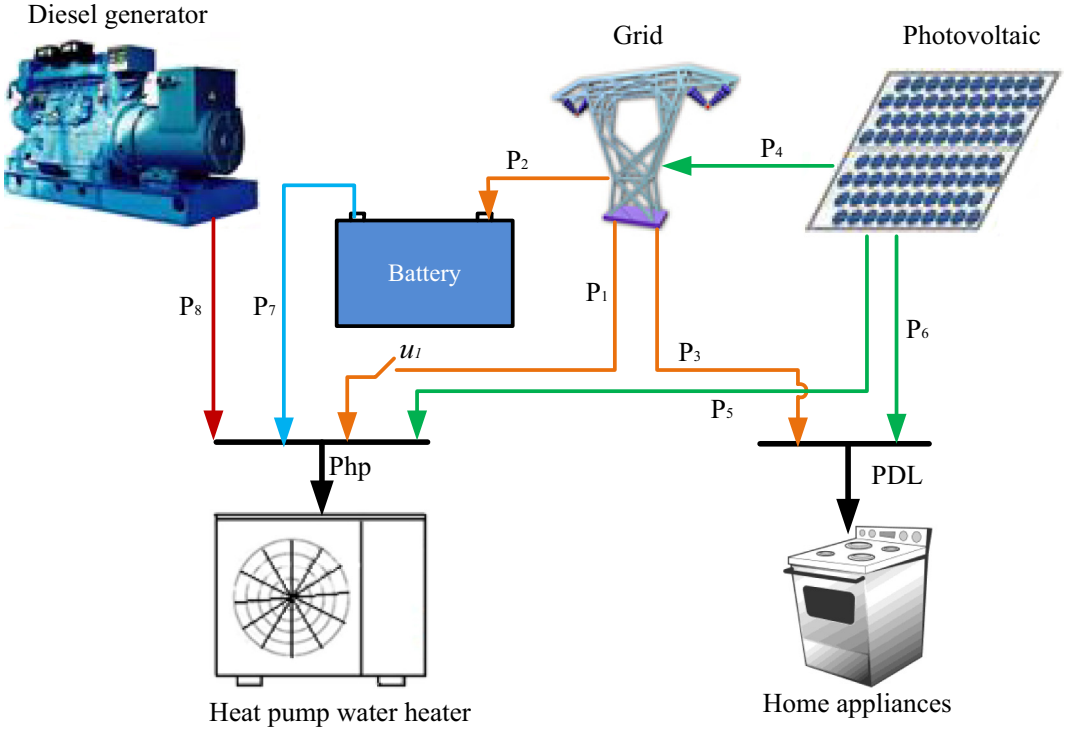

Fig. 1. Schematic layout of the model.

running below 30% of its rated power. The fuel consumption of the diesel generator F in (l/h) is modeled according to Ashok (2007), as shown in Eq. (1), where P is the power delivered and C_f is the fuel price (R/l).

$$F = C_f\left(aP^2 + bP + c\right), \tag{1}$$

The generator coefficients a, b and c are obtained from the manufacturer's data; in this model we adopted the coefficient proposed by Dufo-Lopez and Bernal-Agustin (2008), $a = 0.246$ l/kW h and $b = 0.08145$ l/kW h. The DG fuel efficiency, η_g (kW h/l), is given in Eq. (2),

$$\eta_g = \frac{P}{F} = \frac{P}{C_f\left(aP^2 + bP + c\right)}, \tag{2}$$

The DG power output operates within its lower and upper bounds.

$$0 \leqslant P \leqslant P_{dg}^{rated}. \tag{3}$$

where P_{dg}^{rated} is the rated power output of the DG.

2.2.2. Heat pump water heater

The HPWH is modeled as a fixed load at a discrete time interval with respect to the electrical power consumption. The power demand, $P_{hp}(k)$, of the heat pump in this paper is taken to be proportional to the thermal load requirements and inversely proportional to its COP. Hawlader et al. (2001) presented a detailed model of all major heat pump components. However, this paper treated the HPWH demand as input data taken from the measured annual profile in the case study in South Africa. The grid supplies $P_1(k)$ directly through switch $u_1(k)$ to the HPWH. The switch and the continuous variable $P_1(k)$ form a mixed integer nonlinear constraint. The grid's direct supply to the HPWH is restricted by the binary variable switch, $u_1(k)$, which can only be 1 or 0, when On/Off respectively. In addition, the HPWH is supplied by the battery, $P_3(k)$, PV $P_5(k)$ and the backup DG, $P_8(k)$. In this paper, for simplicity we denoted $P_i(k)t_s = P_i(k)$, with $i = 1, \ldots, 9$ the total number of control variables inclusive of the switch $u_1(k)$. The sampling time t_s is one hour, while k is the sampling interval $k = 1, \ldots, N$, with $N = 24$. The HPWH power balance is given in Eq. (4) as:

$$P_1(k)u_1(k) + P_5(k) + P_7(k) + P_8(k) = P_{hp}(k), \tag{4}$$

$$P_{hp}^{min} \leqslant P_{hp}(k) \leqslant P_{hp}^{max}, \tag{5}$$

The generalized coefficient of performance of the HPWH is given in Eq. (6) as:

$$COP = \frac{Q_D}{P}. \tag{6}$$

where Q_D is the total hot water demand; a function of mass and energy balance of the HPWH's evaporator, condenser and hot water storage system. P is the total electrical power input to the HPWH, mainly consumed by the compressor, fan and controller unit.

2.2.3. Photovoltaic

The PV power generation $P_{pv}(k)$ is input data in this model, a variable power source from zero to its maximum rated, as shown in Eq. (8). The PV supplies $P_5(k)$ to the HPWH, $P_6(k)$ to the loads and $P_4(k)$ feed-into the grid. The PV power output balance is shown in Eq. (7).

$$0 \leqslant P_4(k) + P_5(k) + P_6(k) \leqslant P_{pv}(k), \tag{7}$$

$$0 \leqslant P_{pv}(k) \leqslant P_{pv}^{max}. \tag{8}$$

2.2.4. Battery

The battery performance index is the state of energy (SOE) (Belfkira et al., 2011), which depends on the initial state of energy $B_c(t-1)$, which is dependent on charging/discharging of power. The battery SOE model is adopted from Ashok (2007) for any given time t. The power flow from $t-1$ to t is given in Eq. (9), where $t = 1, \ldots, 24$.

$$B_c(t) = B_c(t-1)(1-\sigma) + \eta_c P_2(t) - \eta_d P_7(t), \tag{9}$$

The battery is charged with $P_2(k)$ from the grid, while $P_7(t)$ is the discharged power to the HPWH. The stored energy is made available during peak demand and whenever it is uneconomical to use the grid, PV or DG energy. The self-discharged factor σ and the inverter efficiency are neglected in this paper. η_c and η_d are the battery charging (set at 100%) and discharging (85%) efficiency respectively. Here $B_c(t)$ is battery SOE in (kW h) and $\tau = 1, \ldots, k$, therefore, from Eq. (9) the generalized discrete battery dynamics is expressed as:

$$B_c(k) = B_c(0) + \eta_c \sum_{\tau=1}^{k} P_2(\tau) - \eta_d \sum_{\tau=1}^{k} P_7(\tau), \tag{10}$$

However, the utilization of the battery must be within its nominal range, the minimum state of energy B_c^{min} is set to 50% and the maximum B_c^{max} is equal to the battery capacity to prolong the battery life.

$$B_c^{min} \leqslant B_c(k) \leqslant B_c^{max}. \tag{11}$$

2.2.5. Power grid

The grid is modeled as an infinite busbar capable of simultaneously supplying and accepting power from the DREs. The TOU electricity tariff is factored in the model, which is one of the most important optimal control parameters. In South Africa, Eskom is the main power supply utility company, which has a dynamic pricing system $p(t)$ or rather TOU tariff: off-peak (p_o), standard (p_s) and peak (p_p). In this study, the recent Eskom[2] megaflex active energy-TOU tariff was used. In this model p_c is used to denote the PV feed-in tariff at 3.94 R/kW h.[3] The Eskom TOU electricity tariff is:

[2] http://www.eskom.co.za/.
[3] https://energypedia.info/wiki.

$$p(t)=\begin{cases} p_o = 0.3656\,\mathrm{R/kW\,h} & \text{if } t\in[0,7]\cup[23,24],\\ p_s = 0.6733\,\mathrm{R/kW\,h} & \text{if } t\in[7,8]\cup[11,19]\cup[21,23],\\ p_p = 2.2225\,\mathrm{R/kW\,h} & \text{if } t\in[8,11]\cup[19,21], \end{cases} \tag{12}$$

where R is the South African rand and time t is the whole period of the day with $t = 0,\ldots,23$.

2.2.6. Domestic appliance

The domestic appliances P_{dl} are modeled to be the total energy consumed by all other loads in the building except the HPWH and constitute input data for that period.

$$P_3(k) + P_6(k) = P_{dl}(k). \tag{13}$$

2.3. Objective function

The objective function is expressed in a discrete-time domain to minimize energy and fuel cost while maximizing the usage of the greener and cheaper energy whenever available. The DG comes on only when the PV and grid energy proves to be uneconomical. The TOU electricity tariff and the feed-in tariff are one of the important control parameters. The weighting factor ω_j is adjusted based on the desired effects (e.g. savings on energy or maximum rebate) of the customer, $j = 1,\ldots,3$. The sampling time t_s is one hour and the sampling interval $k = 1,\ldots,N$ where $N = 24$.

Objective function:

$$J = t_s\left(\omega_1 p(t)\sum_{k=1}^{N}(P_1(k)+P_2(k)+P_3(k)) + \omega_2 C_f\sum_{k=1}^{N}\left(aP_8^2(k)+bP_8(k)+c\right) - \omega_3 p_c\sum_{k=1}^{N}P_4(k)\right), \tag{14}$$

subject to the following constraints:

$$0 \leqslant P_8(k) \leqslant P_{dg}^{rated}, \tag{15}$$

$$P_1(k)u_1(k) + P_5(k) + P_7(k) + P_8(k) = P_{hp}(k), \tag{16}$$

$$P_{hp}^{min} \leqslant P_{hp}(k) \leqslant P_{hp}^{max}, \tag{17}$$

$$0 \leqslant P_4(k) + P_5(k) + P_6(k) \leqslant P_{pv}(k), \tag{18}$$

$$0 \leqslant P_{pv}(k) \leqslant P_{pv}^{max}, \tag{19}$$

$$B_c(k) = B_c(0) + \eta_c\sum_{\tau=1}^{k}P_2(\tau) - \eta_d\sum_{\tau=1}^{k}P_7(\tau), \tag{20}$$

$$B_c^{min} \leqslant B_c(k) \leqslant B_c^{max}, \tag{21}$$

$$P_3(k) + P_6(k) = P_{dl}(k). \tag{22}$$

where $p(t)$ and p_c are the TOU electricity tariff and the PV feed-in tariff (R/kWh) respectively.

2.3.1. Control variables

This optimization problem is nonlinear, having binary and continuous variables. The continuous variables are the power flows $P_1(k)$, $P_2(k)$, $P_3(k)$, $P_4(k)$, $P_5(k)$, $P_6(k)$, $P_7(k)$ and $P_8(k)$. The binary variable is the switch $u_1(k)$, which assumes the values of 1 or 0, when On/Off respectively. The SOE is the state variable. The upper and lower bounds of the continuous variables are given in Eq. (23) for every kth sampling interval. The continuous variables are $P_i(k)$, where $i = 1,2,\ldots,8$.

$$P_{(i)}^{min} \leqslant P_i(k) \leqslant P_{(i)}^{max} \tag{23}$$

2.4. Mixed integer nonlinear programming

This model contains linear and nonlinear constraints. The binary constraint is the switch $u_1(k)$ that controls the direct power supply $P_1(k)$ to the HPWH. This problem therefore becomes a mixed integer nonlinear one formulated according to Belotti et al. (2013). An additional MINLP optimization solver *OPTI toolbox* in MATLAB was used.

The general *OPTI toolbox* algorithm solver is formulated as follows:

$$min_x\ f^{T_x}\ \text{subject to}\begin{cases} A\cdot x \leqslant b\\ Aeq\cdot x = beq\\ lb \leqslant x \leqslant ub\\ c(x) \leqslant d\\ c_{eq}(x) = d_{eq}\\ c(x) \leqslant d\\ x_i \in z\\ x_j \in \{0,1\} \end{cases} \tag{24}$$

f^{T_x} is the scalar function to be minimized, containing the nonlinear objective function, which is subject to the following constraints:

Linear equalities:
Aeq is a $k \times n$ sparse matrix, beq is a $k \times 1$ vector.
Linear inequalities:
A is a $m \times n$ sparse matrix, b is an $m \times 1$ vector.
Decision variable bounds:
lb and ub are $n \times 1$, indicating the lower and upper bound respectively.
Nonlinear inequalities:
c is a $u \times 1$ vector of functions containing inequality constraints, d is a $u \times 1$ vector.
Nonlinear equalities:
ceq is a $v \times 1$ vector of functions containing nonlinear equality constraints, deq is a $v \times 1$ vector.
Integer constraints:
x_i are decision variables, which must be an integer number z.
Binary constraints:
x_j are decision variables, which must be a binary number $(0,1)$, where $i \neq j$.

2.5. Case study

A case study is done on a 3×16 kW HPWH installed at the Pretoria Hotel in South Africa. The energy consumption of the HPWH was measured at hourly intervals for

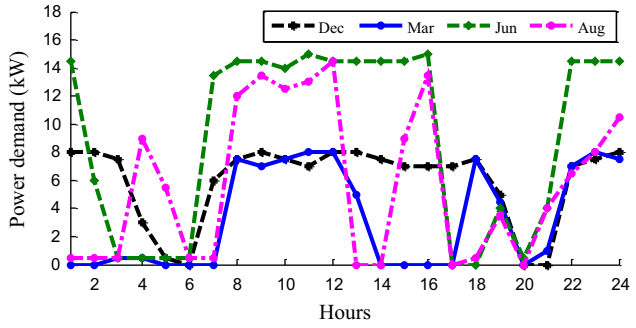

Fig. 2. HPWH hourly demand (kW).

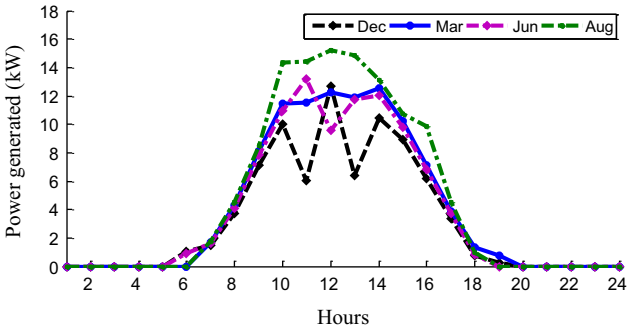

Fig. 3. PV power output (kW).

a year in order to account for seasonal and temperature variations. Fig. 2 shows the hourly demand of the HPWH in (kW) on the selected date in the case study. The other domestic loads were measured as well. The months in the case study were selected in such a way as to match each season in South Africa. The baseline is the current situation at the hotel, where the grid meets the requirements of both the HPWH and domestic appliances. This model proposes an OC strategy intervention to realize cost and energy savings at this hotel, with a possibility of transforming it into an NZEB. This model yields significant savings, as presented in Section 3.

The input data on the PV power generation shown Fig. 3 were adopted from the measured data from our on going research (Tazvinga et al., 2014) on PV models mounted on tilted rooftop. The month of December is observed to illustrate erratic PV power generation because of cloud cover and rain in South Africa.

The deep cycle battery SunXtender[4] type-PVX-2580L was used, with a total capacity of 3×165 A h. The battery capacity was specifically undersized to reduce the initial investment cost and to hold only enough power to supplement the grid during peak demand. During the off-peak period the grid charges the battery with cheaper energy and it makes this cheaper stored energy available to the HPWH and load when needed. The initial SOE of the battery was assumed to be $B_c(0) = 0.5B_c^{max}$.

Diesel Generator BP20S[5] with a maximum power output of 22 kV A, 230 V at 1500 rpm. The current diesel fuel pump price in South Africa is R13.3/l.

2.5.1. Uncertainty analysis of the experimental data

In order to ascertain the confidence level of the measured demand of the heat pump water heater in this case study, the uncertainty error analysis was performed. There is no single method of determining uncertainty error, several techniques exist in assessing uncertainty of the experimental measurement and results. Some methods require knowledge of the system's mathematical model (Esen et al., 2006) and independent variables. Uncertainty analysis is a vital tool at every planning stage of an experiment, it assesses the viability of the outcomes. However, in this paper we used the approach presented in Tungadio and Numbi (2015) to analyze the uncertainty of the experimental data according to Eq. (25). The random error (noise) with an instrument's absolute uncertainty is initialized in the experimental (measured) values. The true (accepted) values are then estimated from the measured (corrupted) values. The difference between true values and the corrupted values, is that the corrupted values are assumed to contain noise resulting from systematic errors especially random errors.

The random errors is generated using Matlab with a distribution mean of 0 and standard deviation equal to 1 which is multiplied by the instrument's absolute uncertainty $\sigma_{m,meas} = \pm 0.01$ given by the manufacturer.

$$Z_m = A_m + RAND_m * \sigma_{m,meas}. \tag{25}$$

where: Z_m is the measured (corrupted) or experimental value of mth measurement; A_m is the true value while $RAND_m$ is the random noise; $\sigma_{m,meas}$ is the standard deviation of the mth measurement and $m = 1, \ldots, 24$ the number of measurement.

The month of December was sampled to analyze the uncertainty of the measured data and the results are shown in Table 1. A simple visual inspection of the true values, show the results are in close agreement with the measured values with a higher confidence level.

Further analysis is carried out to determine the relative uncertainty of each measurement.

$$\text{Relative uncertainty } (\%) = \frac{\text{Absolute uncertainty}}{\text{Measured value}}. \tag{26}$$

The weakest link rule[6] is applied, the measurement with the largest relative uncertainty is picked from Table 1. The largest relative uncertainty which is the weakest link is used

[4] http://www.sunxtender.com.
[5] http://www.bundupower.co.za.
[6] http://www2.fiu.edu/dbrookes/ExperimentalUncertaintiesCalculus.pdf.

Table 1
Uncertainty error of the measured demand of the HPWH for the month of December.

m	Measured (corrupted) value	Random error	Value (with absolute uncertainty)	True (accepted) value	Relative uncertainty
1	8	0.5688	(8 ± 0.01)	7.421	0.125%
2	8	0.1622	(8 ± 0.01)	7.828	0.125%
3	7.5	0.1656	(7.5 ± 0.01)	7.324	0.133%
4	3	0.6892	(3 ± 0.01)	2.301	0.333%
5	0.5	0.229	(0.5 ± 0.01)	0.261	2.000%
6	0	0.5383	(0 ± 0.01)	-0.548	–
7	6	0.1067	(6 ± 0.01)	5.883	0.167%
8	7.5	0.8173	(7.5 ± 0.01)	6.673	0.133%
9	8	0.2599	(8 ± 0.01)	7.730	0.125%
10	7.5	0.1818	(7.5 ± 0.01)	7.308	0.133%
11	7	0.8693	(7 ± 0.01)	6.121	0.143%
12	8	0.853	(8 ± 0.01)	7.137	0.125%
13	8	0.4018	(8 ± 0.01)	7.588	0.125%
14	7.5	0.1839	(7.5 ± 0.01)	7.306	0.133%
15	7	0.9027	(7 ± 0.01)	6.087	0.143%
16	7	0.3377	(7 ± 0.01)	6.652	0.143%
17	7	0.7803	(7 ± 0.01)	6.210	0.143%
18	7.5	0.0965	(7.5 ± 0.01)	7.394	0.133%
19	5	0.5752	(5 ± 0.01)	4.415	0.200%
20	0	0.8212	(0 ± 0.01)	-0.831	–
21	0	0.6491	(0 ± 0.01)	-0.659	–
22	7	0.547	(7 ± 0.01)	6.443	0.143%
23	7.5	0.6868	(7.5 ± 0.01)	6.803	0.133%
24	8	0.7802	(8 ± 0.01)	7.210	0.125%

to perform the calculation, to determine the final performance index's absolute uncertainty. The performance index in this case is the energy cost.

The performance index of this model is run using the true values A_m to further give confidence of the results. The true value simulation results are presented in Table 3.

3. Simulation results and discussion

3.1. Optimal control strategy of the heat pump water heater and domestic load – December

The optimal control results in Fig. 4 show the power scheduling to the HPWH and the domestic loads December. The TOU electricity tariff legend in Fig. 4(c) applies to all figures in this paper. In Fig. 4(a), the battery P_7 supplied most of the load demand from midnight to the beginning of the morning peak period. The direct grid supply P_1 in Fig. 4(b) to the HPWH only came in for few hours after midnight and at the end of the evening standard TOU period. The OC during a certain period turned *On* the switch; though very little power was consumed, the schedule opted to keep the grid on standby. The optimal switching avoided the peak period to save on energy cost and instead used the cheaper-to-buy battery-stored energy.

The DG supply P_8 in Fig. 4(a) came into supply to assist the PV P_5 during the morning and evening peak periods. The rest of the day the DG was off. The PV P_5 sustained most of the morning peak demand with supplement power from the DG. In Fig. 4(d) the battery SOE is observed to decline owing to the depletion of the stored off-peak energy in the battery. The optimal control could not charge the battery using peak TOU tariff to save on cost. The charging activities resumed immediately after peak demand and the battery SOE increased. The battery resumed supplying P_7 to the HPWH in the standard period, taking over from the PV. The OC in the standard TOU period reduced the usage of the PV power to supply the load. Instead it opted to sell P_4 to the grid, as shown in Fig. 4(c). This action was more profitable according to the cost function.

3.2. Optimal control strategy of the heat pump water heater and domestic load – March

Fig. 5(a) shows that the power demand of the HPWH was lower when compared to December. The battery P_7 met all the demand from midnight to 08:00, though at the beginning of the standard TOU the DG came in and operated till the end of the morning peak period. During the peak period the PV P_7 became the main source and sustained the supply of power till 13:00. In Fig. 5(b) the grid P_1 was completely off from midnight till 18:00 when the PV generation started declining. The grid supplied thereafter for an hour in the evening standard period and avoided the peak period. Th OC switched brought it in again past 22:00 to complement the battery. March has relatively fair weather conditions with less cloud cover than December.

The domestic load in Fig. 5(c), was met by the grid P_3 from midnight to 07:00; thereafter the PV P_6 supplied power the rest of the morning and up to the evening. The optimal schedule sold most excess PV P_4 energy to the grid.

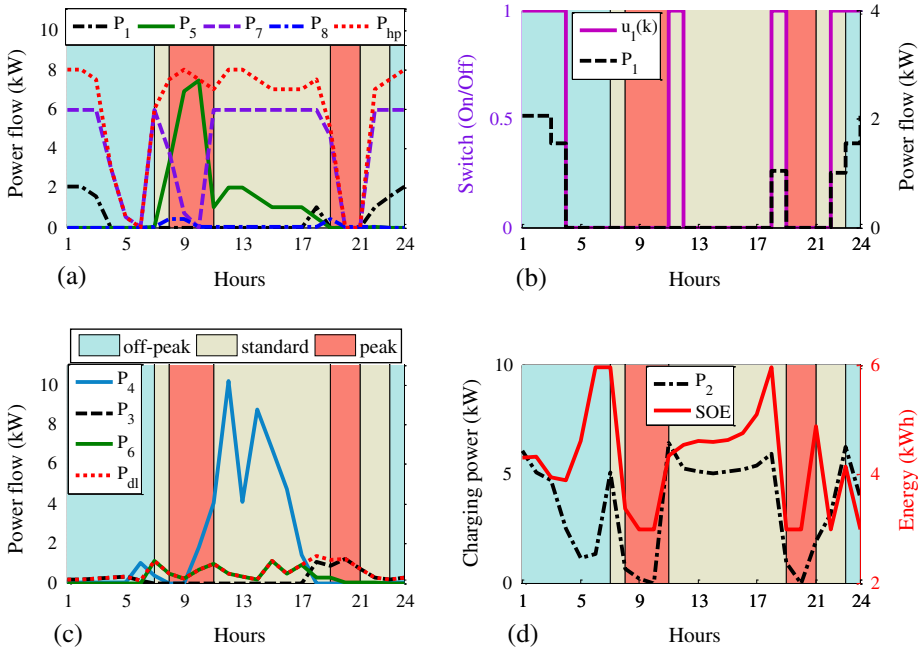

Fig. 4. (a) OC of power to the HPWH; (b) OC switching to the HPWH; (c) domestic load and solar sales; and (d) battery SOE.

This was possible because of low load demand in March. The SOE in Fig. 5(d) shows the battery storing energy from midnight till the beginning of the morning standard TOU tariff period. There was less charging P_2 activity most of the day.

3.3. Optimal control strategy of the heat pump water heater and domestic load – June

June in Fig. 6(a), unlike all other months, falls in winter in this case study. The thermal requirement is usually high, for bathing and space heating. The battery P_7 supplied the HPWH from midnight till the early morning, with minor grid P_1 support. The DG P_8 came in only at 07:00 concurrently with the solar PV P_5 when it began power generation, to complement the battery. The OC dropped P_1 at the approach of the standard TOU period to avoid using expensive energy. The switching frequency increased, as indicated in Fig. 6(b), because of high load demand. The grid P_1 supplied part of the standard periods. The scheduling, however, did not bring in the grid in the evening peak period because the battery had stored enough energy to meet the HPWH demand, supplemented by the DG.

The power scheduling in Fig. 6(c) shows the domestic load supplies. The grid supply P_3 met the load demand from midnight till morning peak. However, the grid was dropped during the peak period and PV P_6 came into sustain the load. There were relatively low solar energy sales P_4 in this month owing to higher load demand. The battery-charging activity is shown in Fig. 6(d); the battery stored energy prior to the beginning of the morning standard period is shown by the SOE upward trend. The sharp fall of SOE in the peak period is due to the switching off the direct grid supply to the HPWH. The strategy was similar in the evening peak period.

3.4. Optimal control strategy of the heat pump water heater and domestic load – August

The optimal control strategy illustrate in Fig. 7(a) followed a similar pattern to the other months discussed above. The DG only supplied power during the morning peak period and the rest of the day it was off. The HPWH's operation was observed to oscillate; this was just the hotel's thermal usage on the selected day. The optimal schedule prioritised the battery's stored energy and the solar energy to supply the loads.

August had the highest solar irradiance in this case study, as shown Fig. 3 above. The solar energy sales were high at midday, though much of the PV-generated energy went to meet load demand.

3.5. Baseline and optimal energy costs

The daily energy and cost savings are presented in Table 2. Baseline cost is the bill which the hotel pays in the case study before the OC intervention while the optimal cost is the bill after OC intervention. This bill is for the grid energy consumed by the domestic load, HPWH and battery charging. The PV energy sales is the generated revenue from sales to the grid.

The energy saved, on the other hand, represents the grid power-not-delivered (energy-not-served) to the load, which would have been delivered without the OC intervention of

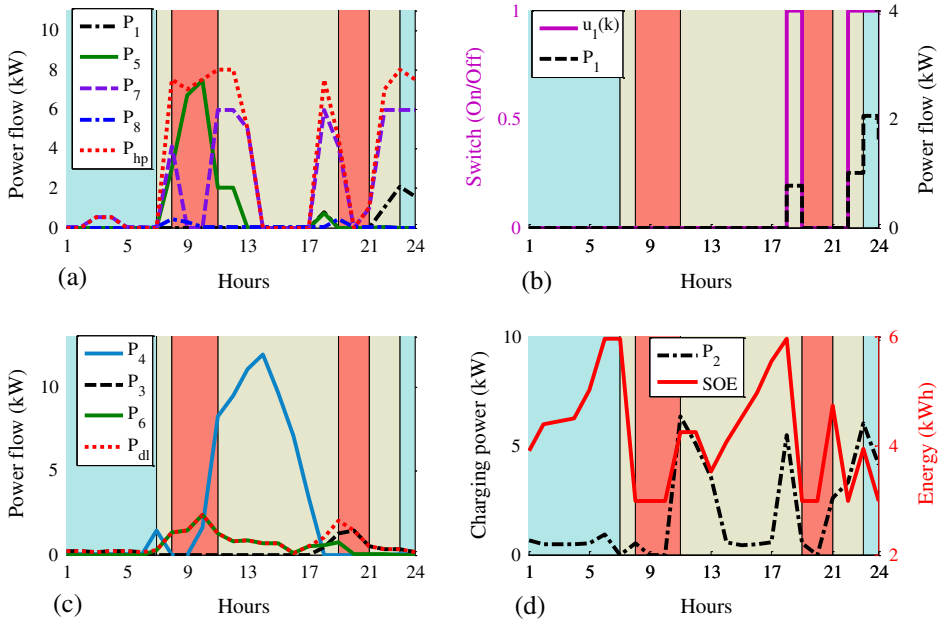

Fig. 5. (a) OC of power to the HPWH; (b) OC switching to the HPWH; (c) domestic load and solar sales; and (d) battery SOE.

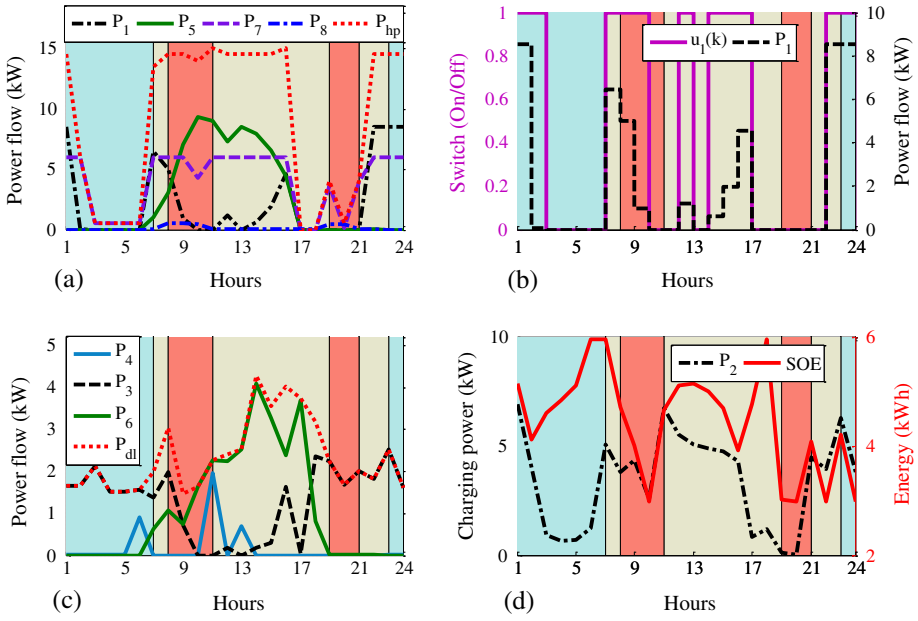

Fig. 6. (a) OC of power to the HPWH; (b) OC switching to the HPWH; (c) domestic load and solar sales; and (d) battery SOE.

this model. This energy is the difference between the baseline and the energy saved owing to the OC strategy. This energy-not-served directly translates into a relief on the utility company's primary input (e.g gas, coal, biomass, nuclear energy, water) in power generation. The reduction in primary energy input helps to mitigate climate change and greenhouse gases emission. However, these impacts are not considered in this paper. The results in Table 2 show the energy and cost savings per day on the selected dates in the case study.

The maximum cost saving was in March, with 68.09%, and a corresponding energy saving of 114.06 kW h in August. The OC strategy is beneficial to the building owner; for example, in March, with baseline cost of R113.94/day the bill after optimization reduced to R36.36/day, translating into a cost saving of 68.09%. The monthly energy cost can be found by multiplying the calender days of each month. The optimal schedule presented a huge benefit, especially with the proposed battery connection model that acts as storage of off-peak energy. The

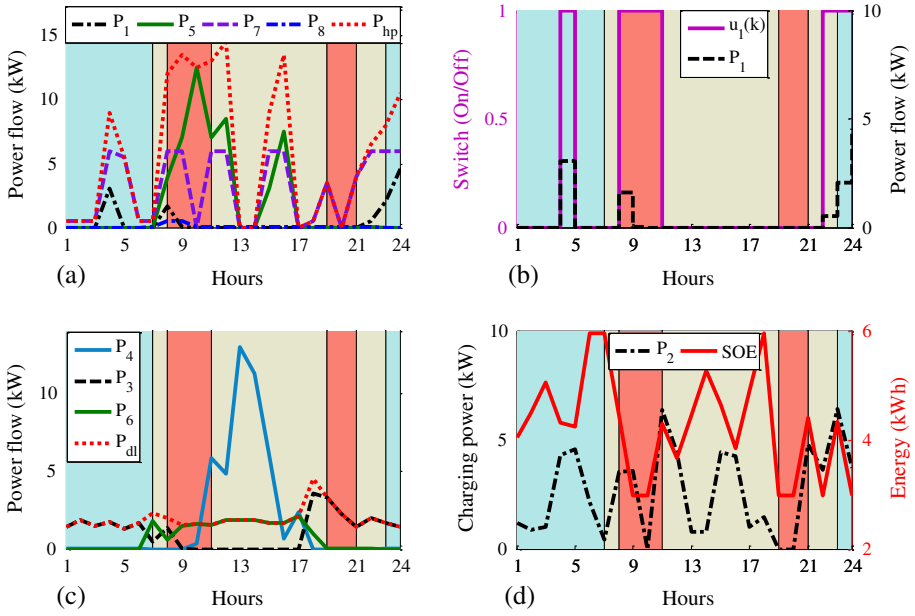

Fig. 7. (a) OC of power to the HPWH; (b) OC switching to the HPWH; (c) domestic load and solar sales; and (d) battery SOE.

Table 2
Daily optimal energy and cost savings.

Month	Baseline cost (R/day)	Optimal cost (R/day)	Solar sales (R/day)	Baseline energy (kW h)	Energy saved (kW h)	Cost savings (%)
December	140.52	62.79	170.02	155.95	80.01	55.32
March	113.94	36.36	251.22	96.76	98.56	68.09
June	253.97	129.48	13.96	274.85	95.69	49.02
August	190.19	79.33	174.32	184.11	114.06	58.29

Table 3
Uncertainty error of the performance index using measured true value.

December	Baseline cost (R/day)	Optimal cost (R/day)	Solar sales (R/day)	Baseline energy (kW h)	Energy saved (kW h)	Cost savings (%)
Experimental value	140.52	62.79	170.02	155.95	80.01	55.32
True value	140.52	58.08	188.17	155.95	79.92	58.67

optimal control strategy achieved both energy and cost savings. Strictly speaking this model is cost-positive on certain days of the month, the income from the solar energy sales can offset the energy bill (e.g. December).

Table 3 below shows the uncertainty error analysis of the model, the month of December was sampled. The percentage error is 5.7% when using the true values. From the results in Table 3 of the measured and true value, conclusion is drawn that uncertainty analysis for the rest of the months in the case study are within the range of December's relative uncertainty.

The experimental measurements and true values used in this model are generally in agreement with each other. The performance index using true values is higher by 5.7%. The total cost saving is R140.52–R62.79 = R77.73/day, therefore, the performance index is multiplied by the largest relative uncertainty (77.73)(0.02) = 1.555. The final absolute uncertainty of the model on cost saving = R(77.74 ± 1.55)/day.

4. Conclusions

The optimal control strategy proposed in this paper achieved huge savings both on energy and cost. The OC opted to use the stored off-peak energy in the battery and minimized the DG operation to the peak period only. The model has the potential to save up to 114.06 kW h of energy daily, with a maximum cost saving of 68.09%. The higher cost saving is owed to the battery connection model being used only as storage of cheaper-to-buy grid energy. The TOU electricity tariff played an important part in the further reduction of energy cost because the battery could be charged in off-peak TOU. This model enables

building owners to trade off solar energy in return for incentives.

The payback period could be shorter owing to huge revenues from the solar energy sales. In addition to the benefits mentioned above in this case study, Eskom gives a rebate upon replacement of resistive element heaters (geysers) with a HPWH, which is not considered in this paper. In respect of the global call for climate change awareness most building owners are now looking for energy-efficient and sustainable technologies. Though this model presents optimal control solutions on energy and cost savings, future work should look into integration of other DREs (e.g. biomass, wind) to supply specifically domestic energy-efficient loads such as HPWHs. This will contribute to the improvement of the utility's power reserves and security of supply through individual participation at building level.

This model is suitable for application in both urban and rural areas. Among its advantages is its suitability for regions with intermittent power supplies. Clearly this model surpasses the solar thermal heater's limitations in terms of space and water heating. The solar thermal heater is too dependent on buildings' architectural design, roof strength and the sun's position, making it difficult to retrofit into existing old buildings. This OC strategy could be adopted for energy/cost saving and by individuals intending to turn their dwelling into zero/energy-positive building. It has proven to be cost-positive on certain days.

References

Ahmad, M.W., Eftekhari, M., Steffen, T., Danjuma, A.M., 2013. Investigating the performance of a combined solar system with heat pump for houses. Energy Build. 63, 138–146.

Ashari, M., Nayar, C., 1999. An optimum dispatch strategy using set points for a photovoltaic (PV)–diesel–battery hybrid power system. Sol. Energy 66 (1), 1–9.

Ashok, S., 2007. Optimised model for community-based hybrid energy system. Renew. Energy 32 (7), 1155–1164.

Belfkira, R., Zhang, L., Barakat, G., 2011. Optimal sizing study of hybrid wind/PV/diesel power generation unit. Sol. Energy 85 (1), 100–110.

Belotti, P., Kirches, C., Leyffer, S., Linderoth, J., Luedtke, J., Mahajan, A., 2013. Mixed-integer nonlinear optimization. Acta Numer. 22, 1–131.

Chow, T., Bai, Y., Fong, K., Lin, Z., 2012. Analysis of a solar assisted heat pump system for indoor swimming pool water and space heating. Appl. Energy 100, 309–317.

Chua, K., Chou, S., Yang, W., 2010. Advances in heat pump systems: a review. Appl. Energy 87 (12), 3611–3624.

Dagdougui, H., Minciardi, R., Ouammi, A., Robba, M., Sacile, R., 2012. Modeling and optimization of a hybrid system for the energy supply of a green building. Energy Convers. Manage. 64, 351–363.

Dufo-Lopez, R., Bernal-Agustín, J.L., 2005. Design and control strategies of PV–diesel systems using genetic algorithms. Sol. Energy 79 (1), 33–46.

Dufo-Lopez, R., Bernal-Agustin, J.L., 2008. Multi-objective design of PV–wind–diesel–hydrogen–battery systems. Renew. Energy 33 (12), 2559–2572.

Ekren, O., Ekren, B.Y., 2008. Size optimization of a PV/wind hybrid energy conversion system with battery storage using response surface methodology. Appl. Energy 85 (11), 1086–1101.

Esen, M., 2000. Thermal performance of a solar-aided latent heat store used for space heating by heat pump. Sol. Energy 69 (1), 15–25.

Esen, M., Yuksel, T., 2013. Experimental evaluation of using various renewable energy sources for heating a greenhouse. Energy Build. 65 (0), 340–351.

Esen, H., Inalli, M., Esen, M., 2006. Technoeconomic appraisal of a ground source heat pump system for a heating season in eastern Turkey. Energy Convers. Manage. 47 (10), 1281–1297.

Esen, H., Inalli, M., Esen, M., 2007. A techno-economic comparison of ground-coupled and air-coupled heat pump system for space cooling. Build. Environ. 42 (5), 1955–1965.

Hawlader, M., Chou, S., Ullah, M., 2001. The performance of a solar assisted heat pump water heating system. Appl. Therm. Eng. 21 (10), 1049–1065.

Hepbasli, A., Kalinci, Y., 2009. A review of heat pump water heating systems. Renew. Sustain. Energy Rev. 13 (6), 1211–1229.

Ikegami T, Iwafune Y, Ogimoto K. Optimum operation scheduling model of domestic electric appliances for balancing power supply and demand. In: IEEE International Conference on Power System Technology, 2010.

Ikegami T, Kataoka K, Iwafune Y, Ogimoto K. Optimal demand controls for a heat pump water heater under different objective functions. In: IEEE International Conference on Power System Technology, POWERCON 2012, 2012.

Infield, D., Mei, L., Eicker, U., 2004. Thermal performance estimation for ventilated PV facades. Sol. Energy 76 (1), 93–98.

Ji, J., Pei, G., Chow, T.-T., He, W., Zhang, A., Dong, J., Yi, H., 2005. Performance of multi-functional domestic heat-pump system. Appl. Energy 80 (3), 307–326.

Khudhair, A.M., Farid, M.M., 2004. A review on energy conservation in building applications with thermal storage by latent heat using phase change materials. Energy Convers. Manage. 45 (2), 263–275.

Kim, S.-K., Jeon, J.-H., Cho, C.-H., Ahn, J.-B., Kwon, S.-H., 2008. Dynamic modeling and control of a grid-connected hybrid generation system with versatile power transfer. IEEE Trans. Ind. Electron. 55 (4), 1677–1688.

Kjellsson, E., Hellström, G., Perers, B., 2010. Optimization of systems with the combination of ground-source heat pump and solar collectors in dwellings. Energy 35 (6), 2667–2673.

Marszal, A., Heiselberg, P., Bourrelle, J., Musall, E., Voss, K., Sartori, I., Napolitano, A., 2011. Zero energy building – a review of definitions and calculation methodologies. Energy Build. 43 (4), 971–979.

Rahman, M.M., Rasul, M., Khan, M.M.K., 2010. Energy conservation measures in an institutional building in sub-tropical climate in Australia. Appl. Energy 87 (10), 2994–3004.

Rodolfo Dufo-LoŽpez, J.L.B.-A., 2008. Influence of mathematical models in design of PV–diesel systems. Energy Convers. Manage. 49 (4), 820–831.

Rousseau, P., Greyvenstein, G., 2000. Enhancing the impact of heat pump water heaters in the South African commercial sector. Energy 25 (1), 51–70.

Santamouris, M., 2014. Cooling the cities – a review of reflective and green roof mitigation technologies to fight heat island and improve comfort in urban environments. Sol. Energy 103 (0), 682–703.

Scognamiglio, A., Røstvik, H.N., 2013. Photovoltaics and zero energy buildings: a new opportunity and challenge for design. Prog. Photovolt.: Res. Appl. 21 (6), 1319–1336.

Setlhaolo, D., Xia, X., Zhang, J., 2014. Optimal scheduling of household appliances for demand response. Electr. Power Syst. Res. 116, 24–28.

Tazvinga, H., Xia, X., Zhang, J., 2013. Minimum cost solution of photovoltaic–diesel–battery hybrid power systems for remote consumers. Sol. Energy 96, 292–299.

Tazvinga, H., Zhu, B., Xia, X., 2014. Energy dispatch strategy for a photovoltaic–wind–diesel–battery hybrid power system. Sol. Energy 108, 412–420.

Torcellini, P.A., Crawley, D.B., 2006. Understanding zero-energy buildings. ASHRAE J. 48 (9), 62–69.

Trianni, A., Cagno, E., 2012. Dealing with barriers to energy efficiency and SMEs: some empirical evidences. Energy 37 (1), 494–504.

Tungadio, M.S., Numbi, B.P., Siti, M.W., Jimoh, A.A., 2015. Particle swarm optimization for power system state estimation. Neurocomputing 148, 175–180.

Verhelst, C., Logist, F., Van Impe, J., Helsen, L., 2012. Study of the optimal control problem formulation for modulating air-to-water heat pumps connected to a residential floor heating system. Energy Build. 45, 43–53.

Zhang, J., Wang, R., Wu, J., 2007. System optimization and experimental research on air source heat pump water heater. Appl. Therm. Eng. 27 (5), 1029–1035.